Mineralogical Magazine, February 1999, Vol. 63(1), pp. 85–104

A geochemical study of two peraluminous granites from south-central Iberia: the Nisa-Albuquerque and Jalama batholiths

J. A. RAMIREZ

Lyongade 6, 2 tv, 2300 Copenhagen S, Denmark

AND

L. G. MENENDEZ

Dept. de Mineralogía y Petrología, Campus Fuentenueva, 18002 Granada, Spain

ABSTRACT

In this paper we present new petrological and geochemical data for two peraluminous granite batholiths (Nisa Alburquerque and Jalama batholiths) representative of the 'Araya-type' granites of the Central-Iberian Zone. Both granites are composite with several facies (monzogranites and leucogranites) that can be grouped into two main granite units: the external units and central units. Intrusive relationships and lack of geochemical coherence between the central and external units indicate that they are not comagmatic but represent different pulses. The central units of both batholiths are petrologically and geochemically different. On the other hand, external units show a lot of similarities and are the main object of this study. The main characteristics of the external granites can be interpreted in terms of an incomplete fractional crystallization process of early mineral phases (plg + Kf + bt) which probably took place at the level of emplacement. Other possible mechanisms of magmatic differentiation (magma mixing, restite unmixing, sequential melting) can be discarded based on field, petrography and geochemical data. We propose that the 'Araya-type' granites are formed by the intrusion of distinct magma pulses (central and external). Further evolution within each pulse can be due to incomplete fractional crystallization possibly taking place at the emplacement level.

KEYWORDS: Peraluminous, Hercynian, granites, geochemistry, fractional crystallization.

Introduction

THE Central-Iberian Zone (CIZ) represents the axial domain of the Iberian Hercynian massif, in which granitic plutonism and metamorphism are widely developed (Bea *et al.*, 1987). Proterozoic and Palaeozoic metasediments, together with some orthogneisses, were intruded by syn- to post-kinematic Hercynian granitoids that usually display a high degree of peraluminosity (Bea *et al.*, 1987).

In central and southern areas of the CIZ, the 'Araya-type' granites (Corretgé *et al.*, 1985; Bea *et al.*, 1987) are the topic of this study (Fig. 1). These intrusives are two-mica ± cordierite ± tourmaline ± andalusite ± sillimanite ± garnet granites, leucogranites and aplites (Corretgé *et al.*, 1985). The 'Araya-type' granites are generally allochthonous, post-tectonic, zoned, contain large volumes of leucocratic differentiates and can be mineralised (Sn, W ± U ± Li ± P). These rocks have apparently evolved as magmas with low quantities of restitic material; they produce characteristic differentiates that are enriched in phosphorus which is typical of Hercynian peraluminous granites (Bea *et al.*, 1987; Bea, 1993).

After a first period of data collection we now possess new petrological and geochemical information on two representative granite batholiths of the Araya group. In this paper, the external units of these intrusions are compared in order to identify the main differentiation mechanisms responsible for the compositional diversity of this group of granites. Due to the small amount of data collected on these granites so far, knowledge

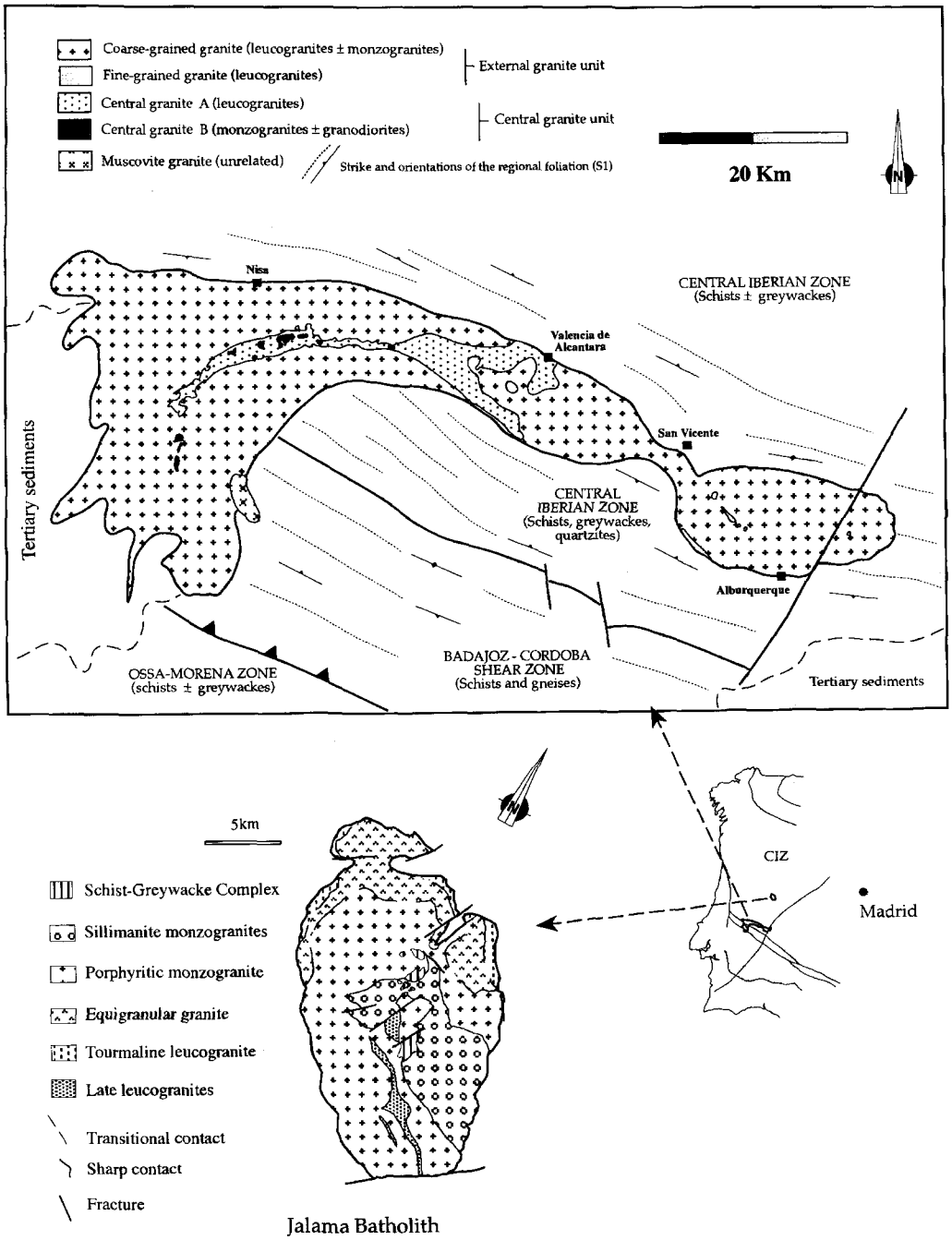

FIG. 1. Geological maps of the Nisa-Alburquerque and Jalama batholiths.

about the petrological processes responsible for their characteristics are poorly constrained as well as their general petrogenesis and significance in the evolution of the Iberian Hercynian massif.

Geological setting

The Araya group of granites is one of the most well exposed in SW Iberia (Corretgé, 1983). It comprises several granitic intrusions emplaced in an epizonal domain of the CIZ, located in the axial domain of the Iberian Hercynian Massif (Julivert *et al.*, 1974). The Araya plutons are allochthonous and post-kinematic (290–250 Ma; Serrano Pinto *et al.*, 1987) with respect to the main phases of Hercynian deformation (Upper Devonian-Middle Carboniferous; Martínez-Catalán, 1990; Díez Balda *et al.*, 1995). They are mainly composed of peraluminous monzogranites and leucogranites, which outcrop in the core of D1 anticlines between NW-SE-trending synclines (Corretgé, 1983; López Plaza and Martínez-Catalán, 1987). Mineral parageneses in the contact aureoles indicate a shallow depth of emplacement ($\approx$2–3 kbar).

The Araya granites are intruded into a group of terrigenous sediments of Upper Proterozoic age, the Schist-Greywacke Complex. Two main formations can be distinguished in this complex: a lower one, mainly pelitic, with thin layers of sandstones, conglomerates, felsic volcanoclastics and amphibolites; and an upper one consisting of slates, mudstones, and siltstones with minor alternations of sandstones, conglomerates and limestones (Rodríguez Alonso, 1985; Díez Balda, 1986; Díez Balda *et al.*, 1995). The base of the Schist-Greywacke Complex does not outcrop in SW Iberia; in a region situated to the west, Ribeiro (1974) observed that it lies unconformably on a gneissic complex.

Field geology and petrogaphy

The Nisa Alburquerque batholith (NAB)

The Nisa Alburquerque batholith (NAB) is a $\approx$1000 km^2 elongated intrusion that is parallel to the SW limit of the CIZ (Fig. 1). Towards the western domains, the intrusion seals the contact of the CIZ domain with the Badajoz-Cordoba shear zone. The NAB intrudes a thick sequence of schists and greywackes (Schist-Greywacke Complex or SGC) of late Precambrian-Cambrian age. To the south-west, the batholith intrudes schists, quartzites and orthogneisses of Palaeozoic ages (from Ordovician to Devonian). Previous studies in the contact aureole developed in the Schist-Greywacke Complex (Suarez Rodriguez, 1985) indicate P–T conditions of 2.3 kbar and 500°C.

Five granitic facies have been distinguished in the NAB (Fig. 1):

(i) Coarse-grained granites (leucogranites ± monzogranites; $\approx$70% of surface outcrop).

(ii) Fine-grained granites (leucogranites; <5% of surface outcrop).

(iii) Aplites (leucogranites; <1% of surface outcrop).

(iv) Central facies A (leucogranites; $\approx$20% of surface outcrop).

(v) Central facies B (monzogranites ± granodiorites; <5% surface outcrop).

The central facies (A and B) consist of a band or large dyke intruded into the coarse-grained granites. This band is composed of A facies, $\approx$75%, (leucogranites) hosting B facies, $\approx$25%, (enclaves of monzogranites ± granodiorites). Contacts between A and B facies are sharp. Fine-grained granites (enclave-like bodies of 10 m^2 to 10 km^2) and aplites (dykes of 0.25–5.00 m thickness) appear always included in the coarse-grained granites, having either gradational (1–10 m transition) or sharp contacts.

On the basis of these relationships we have grouped these facies in two granite units:

1) External granite unit (coarse-grained granites, fine-grained granites and aplites).

2) Central granite unit (central facies A and B).

The external granite unit

The three facies (coarse- and fine-grained granites and aplites) have the same mineralogy (quartz, plagioclase, K-feldspar, biotite, muscovite ± tourmaline, ± cordierite, ± andalusite) and only differ in their modal proportions of varietal minerals (biotite, muscovite, tourmaline, cordierite and andalusite) and in their textures. In general, biotite + muscovite typically form up to 10% of the modal abundance. Tourmaline + cordierite + andalusite typically form <3% of the mode. Andalusite, muscovite, quartz, and tourmaline are mainly late crystallizing magmatic phases.

In the fine-grained facies the amounts of biotite and cordierite are less than in the coarse-grained facies, and muscovite > biotite. In the aplites these amounts are even lower, with muscovite > biotite.

Accessory minerals of external granites (mostly included in bt) are apatite, zircon, monazite and ilmenite. Xenotime ± arsenopyrite occur in the most leucogranitic terms. Rutile ± titanite occur in the most monzogra-

nitic terms. Most of the titanite has a secondary appearance (anhedral shapes and association with other secondary minerals as chlorite and altered ilmenite).

The main difference between facies is textural: the coarse-grained granite can be either porphyritic or equigranular; fine-grained facies and aplites always have an equigranular texture and finer grain size.

In the external granite unit, fine-grained facies and aplites predominate towards the eastern domains of the batholith and coarse-grained granites tend to be more leucocratic towards the east. This reveals a slight E–W zonation in terms of facies distribution and leucogranitic character in the coarse-grained granite.

The central granite unit

Facies A makes up most of the exposed surface of the central granite unit. This is a two-mica leucogranite, with muscovite + biotite <8% and muscovite > biotite. The texture is equigranular and medium-grained. Facies A is fairly homogeneous except towards the most eastern zones and near the contact with the external granites (coarse-grained facies), where it develops a similar mineralogy to that of the coarse-grained facies ($\pm$ tourmaline $\pm$ andalusite $\pm$ cordierite), and the texture becomes somewhat more porphyritic. In these eastern domains and near the contacts, we find textural evidences of mixing between the central leucogranites (A facies) and the external, coarse-grained granite. Some of these evidences are the presence of partially corroded phenocrysts of biotite, plagioclase and K-feldspar in the matrix of A leucogranites.

Facies B is made up of monzogranites $\pm$ granodiorites that appear as enclave-like bodies (5–20 km^2) hosted by the A leucogranites. They are two-mica granites with biotite >> muscovite (biotite $\pm$ muscovite $\approx$10%). Plagioclase is more abundant than K-feldspar. The texture is equigranular and medium-grained. Plagioclase crystals form a network with quartz and K-feldspar occupying the space left (a subophitic-like texture). Accessory minerals (mostly included in biotite) are apatite, monazite, zircon, ilmenite, rutile, titanite $\pm$ epidote. Titanite and epidote both have a secondary appearance in SEM images (anhedral shapes and association with altered ilmenites or plagioclases).

Field relationships between the central and external granite units

The central granite (facies A) displays sharp contacts with the external granite (coarse-grained facies). However, in the most eastern zones of the central band, contacts are transitional (20–30 m width) and outcrop geometry is quite irregular.

The coarse-grained granites have a slight magmatic fabric exhibited by K-feldspar and plagioclase phenocrysts. This fabric can be either parallel or oblique to the contacts with the central granite band. In some local outcrops central facies A crosscuts the magmatic fabric and aplites intruded in the coarse-grained granites.

Near the contacts we find enclaves of external coarse-grained granite inside the central granites but also the reverse relationship (central granite enclaves in the external coarse-grained granite).

In summary, all these relationships, together with the petrographic data, favour a probable intrusion of the central granite (facies A carrying enclaves of facies B) into the external granite (coarse- and fine-grained granites and aplites), a scheme similar to that proposed by Vigneresse and Bouchez (1997) for the Cabeza de Araya pluton. In the eastern domains of the central unit there is a mixing event with the external, coarse-grained granite. This mixing event and the ambiguous enclave relationships indicate that both granites (central and external) were probably magmas with low viscosities at the time of intrusion of the central granite. In the southwest of the batholith there are some enclaves of facies B hosted by the external coarse-grained granite. These present evidence of partial magma mixing and were possibly carried up by the external granite unit during its ascent.

The Jalama batholith (JB)

The JB is a 220 km^2 NW-SE elongate granitic intrusion that outcrops close to the centre of the CIZ (Fig. 1). It displays a considerable lithological variation and is mainly composed of two-mica ($\pm$ sillimanite $\pm$ tourmaline) monzogranites and leucogranites. In the northern third of the pluton, contacts between facies are transitional and parallel to the margins of the intrusion (Fig. 1). In the southern part of the intrusion contacts are sharp, intrusive and parallel to the Hercynian foliation of the wall rocks (Schist-Greywacke Complex). Taking all these relationships into account, two major units have been defined (Ramírez, 1996): a) external granite unit

(equivalent to the external granite unit of the NAB), b) central granite unit.

The external granite unit is made up of three main facies which define a vertical zonation related to the pronounced topographic relief in the northernmost part of the pluton; the sequence from base to top is: porphyritic monzogranite, equigranular granite and tourmaline leucogranite.

1) Porphyritic monzogranite (PM) forms the bulk of the JB and has many similarities with the coarse-grained granite of the NAB. It consists of two-mica monzogranites which are porphyritic, being made up of K-feldspar phenocrysts in a coarse-grained equigranular mesostasis of quartz, plagioclase, K-feldspar, biotite and muscovite (bt $\geqslant$ ms); tourmaline, apatite, ilmenite, monacite and zircon appear as accessory minerals, mainly as inclusions in biotite. Biotite and plagioclase (An_{10-1}) are early crystallizing phases that appear as isolated subhedral crystals or in clusters. K-feldspar is mainly microcline and typically shows inclusions of all the other phases. Quartz is mainly located in the groundmass as anhedral grains, as well as muscovite which appears interstitially.

2) Equigranular granite (EG) outcrops in the northern half of the pluton between the porphyritic monzogranite and the tourmaline leucogranites which form the margins of the intrusion (Fig. 1). It consists of two mica monzo- to syeno-granitic rocks with mineralogies and textures very similar to the mesostasis of the PM, although they lack K-feldspar megacrysts. Muscovite is slightly more abundant than biotite.

3) Tourmaline leucogranite (TL) is restricted to the margins of the pluton, between the EG and the wall rocks. Unlike the other two facies, biotite is absent and tourmaline appears as essential; Li-phosphates are also present. Aplites, pegmatites and Sn and W mineralizations are conspicuously associated with the TL. The texture is medium-grained equigranular; albitic plagioclase (An_{4-1}) is more abundant than K-feldspar.

The central granite unit is made up of sillimanite monzogranites (SM) and late leucogranites (LL), and outcrops as two bands parallel to the elongation of the pluton (Fig. 1). SM is intruded by the porphyritic monzogranite of the external granite unit while the late leucogranites intrude all the rest.

1) The SM is a very heterogeneous unit due to the marked variation with respect to the amount of micaceous enclaves it contains. Two major subfacies can be defined: (i) Enclave-rich monzogranite. It is easily identified by the great abundance of micaceous aggregates it contains, which are up to 5 cm in diameter, mainly composed of primary biotite and sillimanite, and interpreted as restites (Ramirez, 1996). These aggregates present a very well defined crenulation cleavage. The enclave-rich monzogranite is also characterized by a higher proportion of biotite in the groundmass and for being heterogeneously porphyritic with few, but large, megacrysts of K-feldspar. Granodioritic enclaves and quartz globules can be locally observed. The texture is medium-grained porphyritic with biotite in clusters and muscovite containing inclusions of sillimanite. Biotite is more abundant than muscovite. Apatite, zircon, monazite, ilmenite and huttonite have also been identified as accessory phases. (ii) Enclave-poor monzogranite. Unlike the previous variety, this displays a more granitic appeareance since it is richer in quartz and in K-feldspar megacrysts and is more homogeneously porphyritic. Biotitic aggregates are present in lesser amounts. Contact relationships between the two subfacies have not been observed due to the lack of outcrop. Petrographically this facies is very similar to the enclave-rich monzogranite but richer in muscovite.

2) Late leucogranites (LL) outcrop as dykes that intrude the monzogranites in central areas of the pluton (Fig. 1). We have mapped two main bodies, one, of approximately 1 km^2, in central areas of the pluton intrudes the two monzogranitic facies, and the other as a long and narrow band in central parts of the southern half, intruded in the porphyritic monzogranite (Fig. 1); this body presents enclaves of the sillimanite monzogranites although these two lithologies are not found in contact with each other at the present level of outcrop. The LL are similar to the leucogranites of the external granite unit except for the absence of tourmaline and the presence of accessory biotite. Unlike the leucogranites of the external granite unit no mineralizations have been described associated with the LL. The texture is medium- to fine-grained equigranular. Apatite, zircon, monazite and occasional uraninite and Li-Na phosphates appear as accessory minerals.

Geochemistry

Analytical methods

Samples

We collected 63 fresh samples in the NAB and 44 in the JB covering all the unaltered textural

varieties of these batholiths except the pegmatitic ones. Between 10–15 kg were taken for coarse-grained porphyritic varieties, 5–10 kg for equigranular and 2–5 kg for aplites. Crushing was done in two steps: crushing to a grain size of less than 5 mm in a crusher with hardened steel jaws and grinding to a grain size of less than 25 μm in a tungsten carbide jar.

Whole-rock analyses

Major element determinations for the JB samples were carried out by X-ray fluorescence (XRF) at the Department of Earth Sciences, Aarhus University, Denmark, in a Philips PW 2400 and for the NAB samples at Facultad de Geología, University of Granada (Spain). The determinations were carried out on fused beads (1 part (0.75 g) of ignited sample to 5 parts of flux), the mixture ignited at 1250°C for 2×5 minutes. Then at 950°C for 3 hours and this is the value given as LOI. In both cases several international standards were analysed as a check on accuracy, which was satisfactory in both cases. Trace element determinations were carried out by ICP-MS on a PE Sciex Elan 5000 spectrometer at the University of Granada (details are given in Bea *et al.*, 1994*a*). Table 1 shows selected representative whole-rock chemical analyses of the NAB and JB.

Results

Geochemical relationships have been explored through the use of variation diagrams and principal components analysis (PCA; Le Maitre, 1982). PCA was performed on three groups of elements which we classified by their unit of measurement (% and ppm) and their mineralogical expression: major elements (SiO_2, TiO_2, Al_2O_3, FeO, MgO, CaO, Na_2O, K_2O and P_2O_5), trace elements contained in essential minerals (Li, Rb, Ba, Sr, V, Zn, Ga, Nb, Ta, Sn, Tl and Eu) and trace elements contained in accessory minerals (Y, Zr, Hf, U, Th, *REE*). This last distinction is based on the results of a LA-ICP-MS study by Bea (1996) and Ramirez (1996) on samples from both batholiths. Original raw data were transformed to their logarithms to give equal weight to elements showing variations of the same order of magnitude (Le Maitre, 1982). The results were obtained by applying the matrix of variance-covariance following the method of Wilkinson (1989). Only the first eigenvectors are presented because these explain a sufficient variance as to discard the second eigenvector.

Results for the central units of the NAB and JB will be presented but not discussed in this paper, the reason being the reduced amount of geochemical information available on these units. These data will appear in forthcoming works (Menendez, in prep.; Ramirez, in prep.) where the petrogenesis of each batholith will be treated separately. In the following, we will concentrate on the study of the external units of both batholiths for which, field and petrographical relations indicate a similar petrogenesis. It should be pointed out that the central units of the Araya plutons are specific for each intrusion (e.g. the Cabeza de Araya batholith; Vigneresse and Bouchez, 1997) and therefore not directly comparable, whereas the external units (monzogranite to leucogranite series) characterize all of them and have many features in common (see below).

Major elements

Both the leucogranites and monzogranites are peraluminous (Zen, 1988) with A/CNK (molecular $Al_2O_3/(CaO + K_2O + Na_2O)$) ranging from 1.07 to 1.40 in the NAB, and from 1.16 to 1.35 in the JB. The FeO/(FeO+MgO) relation varies between 0.78 (monzogranites) and 0.98 (aplites) in the NAB, and from 0.52 to 0.82 in the JB. CaO, FeO_t, MgO, TiO_2, and K_2O decrease with increasing SiO_2 while P_2O_5 can be either enriched or depleted (Fig. 2). These fractionation trends are very similar for the two batholiths. In comparison with monzogranites, the leucogranites are more peraluminous, less mafic, poorer in CaO and with higher Na/K ratios. The diagrams of K_2O and CaO *vs.* SiO_2 for the NAB (Fig. 2) reveal a clear lack of geochemical coherence between central and external granite units, each unit defining independent trends.

PCA on data from the external units results in a first eigenvector mainly controlled by oxides with positive load (MgO, TiO_2, FeO_t, CaO and K_2O) (Fig. 3*a*) while negatively loaded oxides (SiO_2, Na_2O and P_2O_5) have less influence. This is because the positively loaded oxides display stronger relative variations than the negatively loaded ones. The first eigenvector is very similar in both batholiths and accounts for a major amount of the variance (85% for the NAB and 95% for the JB).

Trace elements

Sr, Ba, V, Y, Th, Zr, Nb, Pb, and *REE* become depleted with increasing SiO_2. On the other hand,

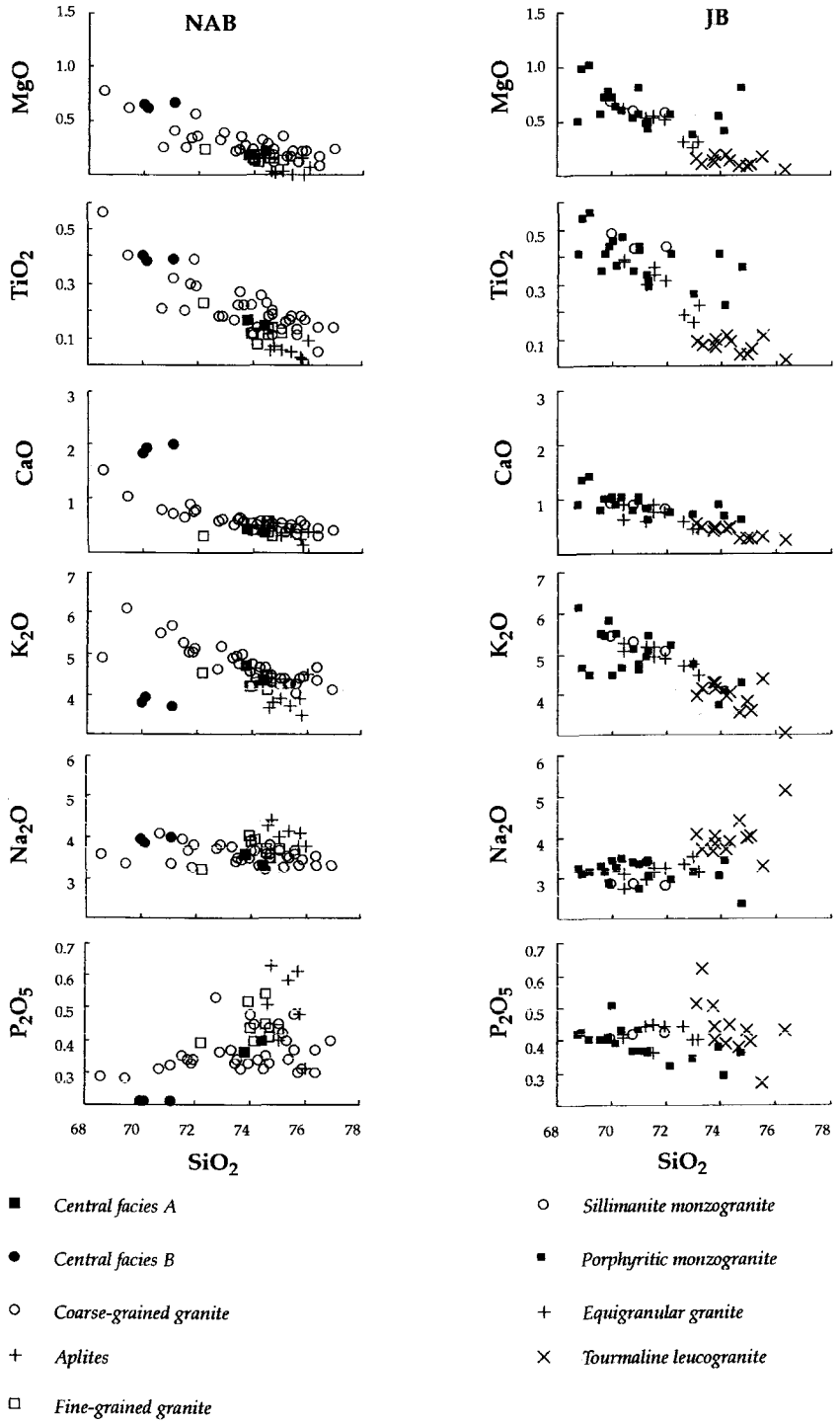

FIG. 2. Major elements variation diagrams of Nisa-Alburquerque and Jalama granites.

TABLE 1. Representative chemical analyses for the NAB (ALL-) and JB (JAL-)

Refs.	ALL-67	ALL-69	ALL 37	JAL-127	JAL-15	ALL 46	ALL 43
Rock type	CGG	CGG	CGG	PM	PM	FGG	FGG
Major elements (%)							
SiO_2	68.56	72.07	75.34	68.73	70.14	74.58	74.55
TiO_2	0.56	0.27	0.17	0.41	0.37	0.11	0.13
Al_2O_3	15.75	14.63	13.02	15.80	15.46	13.94	13.96
Fe_2O_3	2.97	1.64	1.53	2.40	2.13	0.98	1.24
MgO	0.79	0.32	0.18	0.51	0.65	0.16	0.19
MnO	0.02	0.02	0.03	0.04	0.04	0.02	0.02
CaO	1.54	0.56	0.44	0.89	0.90	0.61	0.38
Na_2O	3.60	3.46	3.53	3.26	3.25	3.72	3.62
K_2O	4.92	5.01	4.27	6.13	5.50	4.43	4.10
P_2O_5	0.29	0.37	0.40	0.42	0.39	0.54	0.45
LOI	0.64	0.64	0.74	1.07	1.07	1.03	1.23
Total	99.62	98.99	99.65	99.73	99.93	100.12	99.87
Trace elements (ppm)							
Li	123	196	213	235	260	144	279
Rb	225	330	322	329	360	349	297
Cs	12.3	26.6	20.8	32.3	33.3	44.0	51.4
Be	4.0	6.6	6.3	10.0	10.1	7.9	10.3
Sr	108	36	27	70	98	44	39
Ba	489	142	130	362	320	126	154
Sc	6.0	2.4	3.5	6.3	27.6	6.3	8.1
V	39	16	13	20	19	9	13
Zn	79	63	53	100	89	28	52
Ga	23	20	23	25	20	21	20
Y	17.1	11.3	9.9	18.7	12.7	9.1	6.5
Nb	10.7	8.6	10.2	14.7	16.4	9.3	9.0
Ta	1.1	2.1	1.6	2.1	3.2	2.5	2.9
Zr	96	61	61	106	86	39	43
Hf	2.5	1.9	2.1	3.0	3.0	1.5	1.5
Sn	7.5	16.0	15.7	17.0	19.8	29.2	33.9
Tl	1.5	2.0	2.2	2.0	2.2	2.1	1.8
Pb	27.5	23.4	18.1	37.5	14.4	11.4	19.1
U	3.3	11.7	21.1	7.9	4.4	9.7	6.8
Th	21.0	8.6	7.4	18.7	16.5	1.1	1.5
REE (ppm)							
La	35.64	11.42	12.65	29.07	24.78	4.20	5.26
Ce	77.69	23.41	29.33	72.45	58.86	8.85	10.33
Pr	9.59	3.15	3.50	8.83	7.01	1.09	1.28
Nd	37.85	11.45	13.26	34.04	26.4	3.84	4.56
Sm	7.72	2.80	3.09	7.02	5.35	1.09	1.16
Eu	1.17	0.32	0.30	0.76	0.57	0.27	0.28
Gd	7.31	2.59	2.89	6.27	4.01	1.38	1.33
Tb	0.90	0.41	0.43	0.78	0.56	0.24	0.21
Dy	3.78	2.13	1.99	3.74	2.74	1.56	1.22
Ho	0.65	0.40	0.41	0.7	0.47	0.35	0.27
Er	1.43	1.10	0.94	1.65	1.19	1.01	0.80
Tm	0.18	0.15	0.15	0.24	0.17	0.16	0.12
Yb	1.28	1.01	1.05	1.5	1	1.10	0.83
Lu	0.19	0.17	0.15	0.22	0.14	0.17	0.13

TABLE 1 (*contd.*)

Refs.	ALL 38	JAL-111	JAL-112	ALL-58	ALL-68	ALL 48	JAL-84
Rock type	FGG	EG	EG	AP	AP	AP	TL
Major elements (%)							
SiO_2	75.03	70.38	72.94	75.80	75.08	74.65	73.10
TiO_2	0.12	0.38	0.16	0.02	0.06	0.06	0.09
Al_2O_3	13.51	15.24	14.97	13.83	14.44	13.81	15.24
Fe_2O_3	1.00	2.11	1.27	0.91	0.77	0.82	0.84
MgO	0.15	0.62	0.26	0.01	0.04	0.03	0.15
MnO	0.01	0.02	0.03	0.02	0.01	0.02	0.03
CaO	0.47	0.61	0.44	0.15	0.31	0.46	0.55
Na_2O	3.70	2.73	3.54	4.11	3.98	4.25	4.10
K_2O	4.27	5.27	4.78	3.47	3.87	3.64	3.97
P_2O_5	0.43	0.42	0.40	0.48	0.40	0.51	0.51
LOI	0.91	1.58	1.11	1.17	0.78	0.77	1.14
Total	99.60	99.41	99.93	99.97	99.73	99.02	99.86
Trace elements (ppm)							
Li	204	217	361	407	134	91	484
Rb	311	394	434	456	295	438	518
Cs	33.1	23.6	54.4	22.0	22.8	17.4	97.7
Be	4.3	6.7	8.1	2.1	1.5	2.4	11.7
Sr	36	74	23	2	9	5	52
Ba	135	297	148	0	13	6	41
Sc	5.6	5.2	0.7	1.1	8.5	5.6	6.5
V	9	22	9	8	8	4	6
Zn	48	115	35	42	31	45	73
Ga	20	27	23	28	21	30	28
Y	6.2	12.3	8.3	1.4	3.3	3.0	4.9
Nb	9.0	19.3	12.7	11.8	5.4	13.0	18.8
Ta	2.6	2.7	3.6	2.1	1.0	2.9	7.6
Zr	41	108	48	20	15	20	35
Hf	1.5	3.3	1.8	1.4	0.6	1.3	1.6
Sn	31.0	15.6	28.0	39.1	15.2	22.9	55.8
Tl	2.0	2.3	2.7	3.7	1.7	2.3	3.0
Pb	15.0	30.6	21.0	8.1	15.7	3.8	13.4
U	4.1	7.3	5.2	3.1	3.0	5.1	16.3
Th	1.1	14.4	6.7	2.6	3.0	0.0	3.0
REE (ppm)							
La	3.25	25.5	10.8	1.26	2.54	0.19	5.8
Ce	7.31	59.5	24.9	3.14	4.50	0.03	12.8
Pr	0.90	7.2	3.1	0.35	0.61	0.07	1.2
Nd	3.15	26.9	11.5	0.75	1.88	0.39	4.2
Sm	0.87	5.8	2.8	0.60	0.79	0.16	1.2
Eu	0.26	0.54	0.32	0.02	0.09	0.03	0.13
Gd	1.04	4.9	2.3	0.45	0.71	0.50	0.9
Tb	0.18	0.61	0.33	0.07	0.10	0.09	0.14
Dy	1.21	2.8	1.7	0.41	0.66	0.59	0.9
Ho	0.28	0.45	0.29	0.09	0.13	0.13	0.17
Er	0.81	1.00	0.74	0.26	0.43	0.34	0.42
Tm	0.12	0.13	0.11	0.03	0.06	0.06	0.06
Yb	0.85	0.88	0.68	0.23	0.46	0.40	0.52
Lu	0.13	0.14	0.10	0.05	0.09	0.07	0.07

CGG = coarse-grained granite, PM = porphyritic monzogranite, FGG = fine-grained granite, EG = equigranular granite, AP = aplites and TL = tourmaline leucogranite.

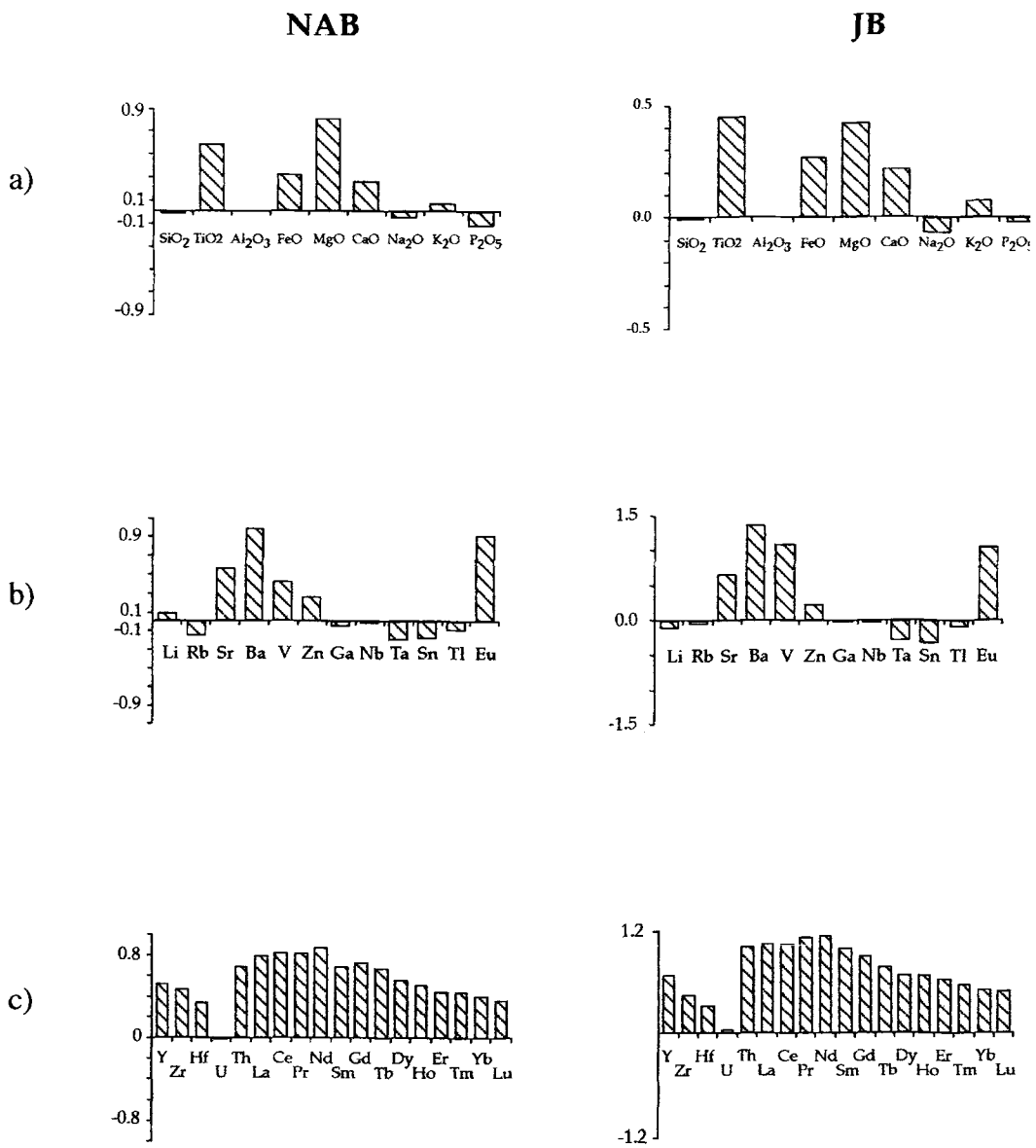

FIG. 3. Component loadings of the first eigenvectors for the Nisa-Alburquerque and Jalama granites; (*a*) major elements, (*b*) trace elements contained in essential minerals, (*c*) trace elements contained in accessory minerals.

Li, Rb, Cs, Be, Ga, Sc, U, Ta and Sn show a tendency to increase with SiO_2, with some scatter in the most leucogranitic terms (Fig. 4). Lack of geochemical coherence is evident between external and central granite units as shown by Sr and Zr for NAB and by Zr for JB (Fig. 4).

PCA on the trace elements contained in essential minerals for data from the external units shows that positively loaded elements (Ba, Eu, Sr, V and Zn in order of magnitude, Fig. 3*b*) have a higher weight in the definition of the first eigenvector than negatively loaded elements. This vector is very

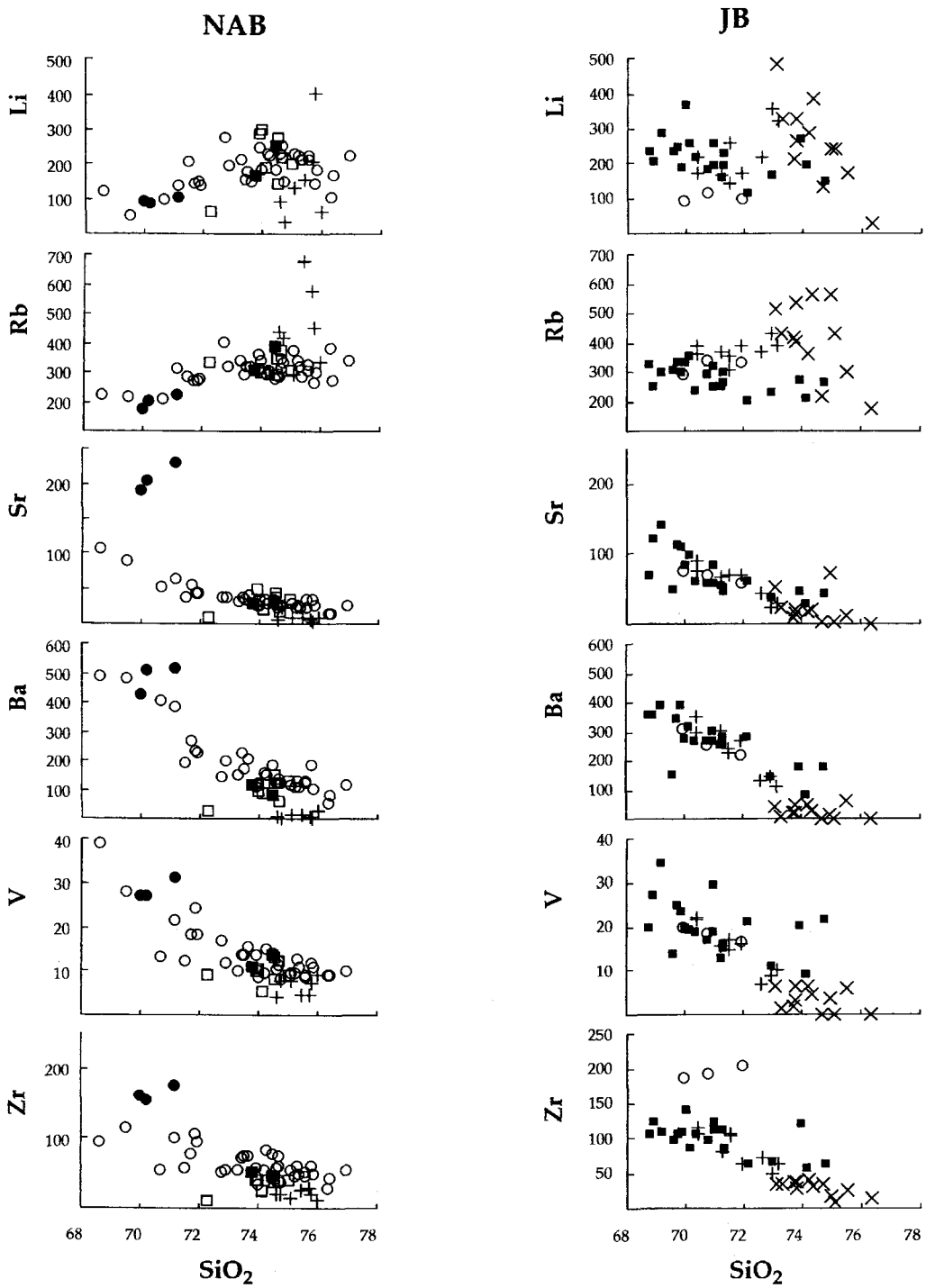

FIG. 4. Trace elements variation diagrams of Nisa-Alburquerque and Jalama granites.

similar in the two batholiths, the only difference being Li, which associates with elements of positive sign in the NAB and negative in the JB. The variance explained by the first eigenvector is 70% for the NAB and 76% for the JB.

With respect to the rare earth elements, monzogranites show the highest ΣREE, fractionated spectra ($La_N/Lu_N \approx 15$) and have a pronounced Eu anomaly ($Eu/Eu^* \approx 0.3$; Fig. 5), reflecting the strong influence that the monazite *REE* pattern exerts on the whole-rock *REE* pattern in peraluminous granites (Bea, 1996). *LREE* concentrations decrease more than *HREE* ones with differentiation, as indicated by the flatter *REE* patterns of the leucogranites compared with those of the monzogranites. Also, the Eu anomaly becomes stronger in the NAB, but is weaker in the JB. For the trace elements contained in accessories, PCA on data from the external units results in a first eigenvector mainly defined by a positive load of all the elements, especially the *LREE*; there are no negatively loaded elements (Fig. 3*c*). The more marked influence of the *LREE* reflects their more pronounced relative variation with respect to the *HREE*, Zr and Y. The amount of variation which can be explained by this vector is very high in both cases (86% for the NAB and 93% for the JB) and there is no difference between the NAB and the JB with respect to the first eigenvector.

Although the two batholiths have similar ranges of concentrations and differentiation trends for many elements, the frequency distributions for most of the elements are very different. In Fig. 6 a comparison of the distribution of some key elements is shown; in the case of SiO_2 the distribution is skewed towards higher values in the NAB than in the JB; the opposite is observed for MgO, V, and Zr. These patterns of distribution reveal that the NAB is more evolved with a higher

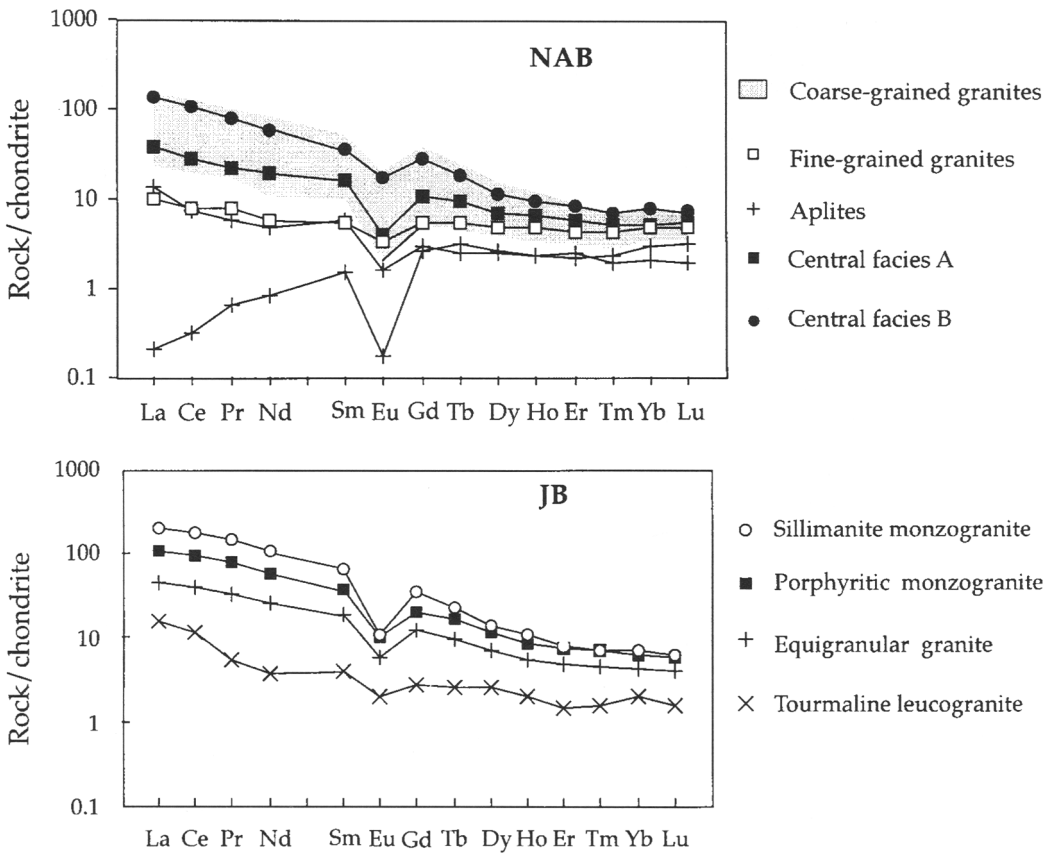

FIG. 5. Chondrite-normalized patterns of *REE* for Nisa-Alburquerque and Jalama granites.

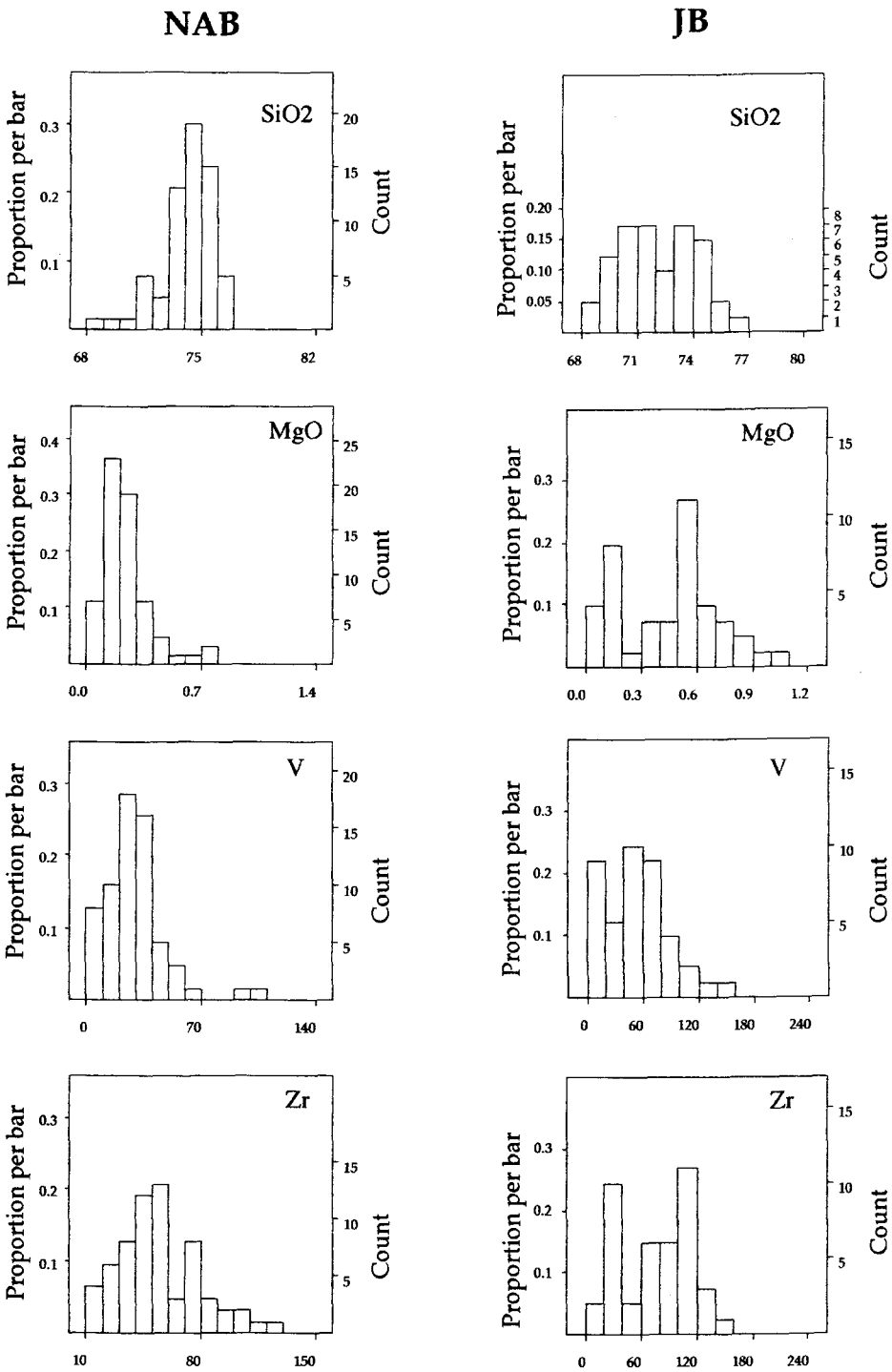

FIG. 6. Histograms of some key elements in NAB and JB.

proportion of leucogranites with respect to monzogranites than the JB.

Discussion

Mechanisms of evolution

Geochemical trends displayed by two-mica granites can result from a variety of processes among which progressive fractional melting (Shearer *et al.*, 1987), variation inherited from partial melting of heterogeneous source rocks (Deniel *et al.*, 1987), restite unmixing (Chappel *et al.*, 1987) and fractional crystallization (Scaillet *et al.*, 1990; Bea *et al.*, 1994*a*) are the most commonly invoked. Other possible processes are magma mixing, assimilation and hydrothermal alteration (Clarke, 1992).

Intrusive relationships and lack of geochemical coherence between members of the central and external units of the NAB and JB suggest that these represent independent magma pulses as already pointed by Ramirez (1996) for the JB. Similar relationships are observed in the Cabeza de Araya pluton (Corretgé *et al.*, 1985) and are thought to be produced by magma pulsing (Vigneresse and Bouchez, 1997). On the other hand, field, petrographic and geochemical relations within the granites that make up the external units of the NAB and JB confirm that these constitute magmatic differentiation sequences. It should be pointed out that Sr isotope compositions are homogeneous (Ramirez, 1996; Menendez, in prep; Bea unpublished data) suggesting a comagmatic relationship between the granite facies that make up the external units. In the following we will concentrate on the discussion of the geochemical variability within the members of the external units of both batholiths. The comagmatic character rules out the processes of magma mixing, assimilation and hydrothermal alteration to explain the origin of the compositional variations. A process of restite unmixing can also be discarded on petrographical grounds since we have not found evidence of restite in our thin sections. Furthermore, the $FeO+MgO+TiO_2$ content in these rocks are equal to, or lower than, the amounts possible to dissolve in a granitic melt (Wall *et al.*, 1987).

Rb-Sr modelling

Compositional trends within the external units of the NAB and JB can be interpreted in terms of either sequential crystallization or sequential melting; a dilemma often encountered in studies of granite petrogenesis (Williamson *et al.*, 1996). In order to distinguish between these two processes we have carried out Rb-Sr modelling for the external units of NAB and JB.

The following equations for crystallization and melting (see Rollinson, 1993 for a review) have been used:

Equilibrium crystallization

$$C_L = C_o/(D + F(1 - D)) \quad (1)$$

Fractional crystallization

$$C_L = C_o F^{(D-1)} \quad (2)$$

Equilibrium melting

$$C_L = C_o (1 - (1 - F)^{(1/D)})/F \quad (3)$$

Fractional melting

$$C_L = C_o (1 - F)^{(1 - D/D)}/D \quad (4)$$

where C_L is the concentration of a trace element in the liquid, C_o is the trace element concentration for the original unmelted solid (partial melting) or for the parental liquid (fractional crystallization), F is the % of melt produced (partial melting) or remaining (fractional crystallization), and D is the bulk partition coefficient for the trace element considered ($D = \Sigma X_i\, Kdi$). Values of Kd used for the modelling are listed in Table 2. C_o values used for both the crystallization and melting models are the Rb and Sr concentration of the least leucocratic monzogranites (ALL-67 and JAL-86). The fractionating assemblage selected is based on modal estimations in the monzogranites (30% plg, 25% Kfs, 5% bt). The residual assemblage is taken from the experiments of Montel and Vielzeuf (1997) (P = 8 kbar, T = 855°C, A109C P (22.1% bt, 30.5% plg, 0.4% grt)

TABLE 2. Crystal/melt distribution coefficients used in crystallization and melting models

Elements	K_d	Reference
Rb in bt	2.240	Arth, 1976
Rb in kfs	0.340	Arth, 1976
Rb in plg	0.041	Arth, 1976
Rb in crd	0.080	Bea *et al.*, 1994*b*
Rb in grt	0.060	Bea *et al.*, 1994*b*
Rb in opx	0.003	Arth, 1976
Sr in bt	0.447	Nash and Crecraft, 1985
Sr in plg	15.633	Nash and Crecraft, 1985
Sr in kfs	5.400	Arth, 1976
Sr in crd	0.012	Bea *et al.*, 1994*b*
Sr in grt	0.010	Bea *et al.*, 1994*b*
Sr in opx	0.009	Arth, 1976

and A115C P (4.1% bt, 23.4% plg, 5.9% opx, 5.4% grt)). The reasons for selecting the compositions used by Montel and Vielzeuf (1997) is because metagreywakes are thought to be a more likely source than metapelites for peraluminous granites (Miller, 1985).

The results of modelling are shown in Fig. 7 for NAB external unit and in Fig. 8 for JB external unit. We have calculated liquid and solid evolution trends and have modelled evolution trends of mixtures of liquids and solids, for a fractional crystalization model (McCarthy and Hasty, 1976). It has to be stressed that these models are based on assumptions of probabilities with considerable uncertainties. This is especially the case for the melting models in which it is neccesary to assume a possible protolith, initial Rb and Sr contents, residual mineral assemblage and $P-T$ conditions of melting. All these parameters are very often impossible to estimate from a study of allocthonous granites.

The main points of the modelling are (Figs. 7 and 8):

For the bulk of samples studied (leucogranites and monzogranites), it is not possible to distinguish between melting and crystallization trends. For melting we have selected the best fitting models and initial Rb-Sr compositions of the least evolved members of NAB and JB (All 67 and Jal 86). This assumption is likely to be different in reality (different initial Rb and Sr in the protolith) and this would cause worse fitting melting models.

In the melting model, melting percentages of up to 80% are necessary to fit most of the compositional range observed in NAB and JB granites. Experimental and theoretical considerations preclude such high melting percentages (i.e. Clemens and Vielzeuf, 1987; Patiño-Douce and Johnston, 1991; Montel and Vielzeuf, 1997). On the other hand, the fractional/equilibrium crystallization model reproduces the compositional range observed very closely.

The most evolved leucogranites, with very low Sr contents, cannot be generated by a sequential melting process, since they are too evolved to have been unmodified crustal melts; such evolved compositions are more likely attained as a result of a fractional crystallization process.

If fractional crystallization is considered as the model that best fits the data, the samples from NAB and JB do not represent pure melts but mixtures between melts and early fractionated crystals (i.e. cumulates). In the case of NAB, the monzogranites would be mixtures of 75% liquid and 25% solid. In the case of JB some of the monzogranites would be 60% liquid and 40% solid. This difference might indicate a better solid-liquid unmixing in the case of JB, or that the fractional crystallization process has been more effective in JB.

Further evidences for a sequential crystallization process

Besides the Rb-Sr modelling shown above, other lines of evidence suggest that the most suitable interpretation to explain the chemical variation within the external units of the NAB and JB is fractional crystallization of early mineral phases:

(1) Temporal relationships between some leucogranites and monzogranites are opposite to those typical of sequential partial melting, which should progressively yield more mafic magmas. In the NAB, some of the fine-grained granites included in the coarse-grained granites show intrusive contacts and relationships indicating a progression with time towards more felsic compositions, a situation consistent with a liquid line of descent toward the granite minimum. Similar relationships between aplites and syeno-monzogranites can be observed in the JB.

(2) Increasing abundance of tourmaline with differentiation points to a progressive enrichment of B in residual melts which is best explained in terms of a fractional crystallization process (Benard *et al.*, 1985).

(3) The low contents in Sr, Ba and Eu in most of the leucogranitic terms, indicate that they cannot be generated directly by partial melting of a source rock capable of producing reasonable amounts of peraluminous leucocratic melts. The impoverishment in these elements can be better explained by fractionation of feldspars.

(4) The more pronounced variation in concentration of the compatible elements than the incompatible are suggestive of a fractional crystallization process (McCarthy and Hasty, 1976; Hanson, 1989).

(5) Experimental results presented by Scaillet *et al.* (1995) demonstrate that fractional crystallization of peraluminous leucogranitic magmas produces derivative liquids that are more peraluminous, less mafic, poorer in Ca and with a higher Na/K ratio than their parental compositions. These fractionation trends are perfectly matched in the monzogranite-leucogranite series of the external units of the NAB and JB. The decrease in

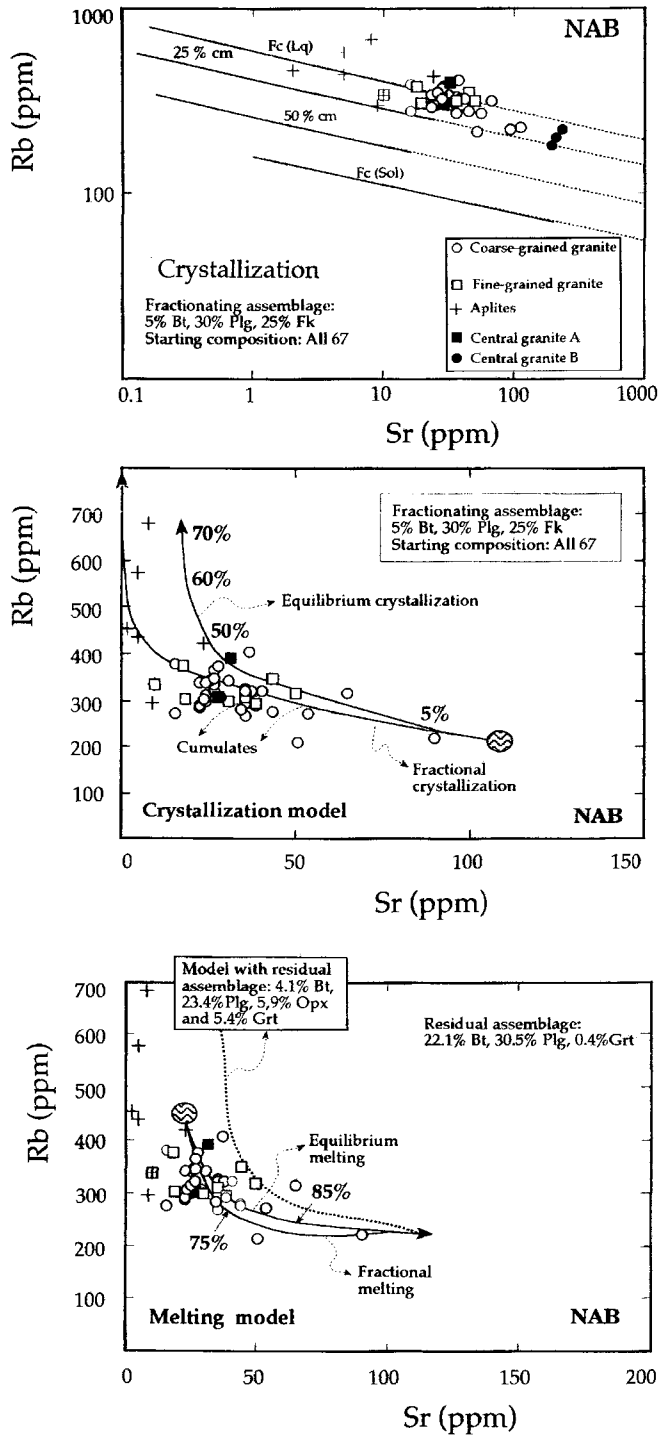

FIG. 7. Results of Rb/Sr modelling for the Nisa-Alburquerque granites.

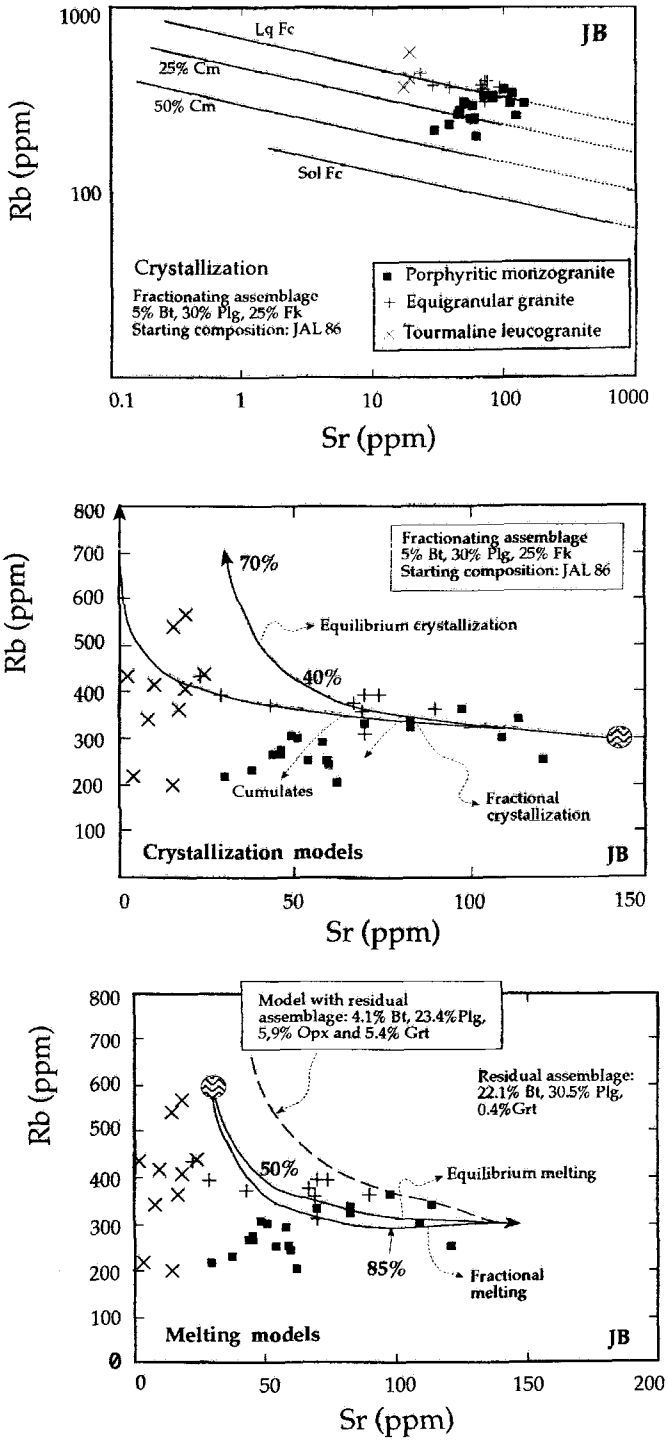

FIG. 8. Results of Rb/Sr modelling for the Jalama granites.

Fe, Mg and Ti with differentiation can be explained by fractionation of biotite, whereas fractionation of feldspars must account for the observed depletion in CaO, Sr, Ba and Eu. Fractionation of biotite leads to that of the accessory phases included in this mineral, mainly monazite, zircon and apatite and therefore, the impoverishment of Zr, Hf, Y, Th and the *REE* (except Eu) is directly correlated to that of the ferromagnesian minerals. In the case of the JB, the Eu anomaly tends to dissappear with differentiation. This can only be explained by the stronger fractionation of monazite and zircon compared to that of feldspars, since these minerals accumulate $\approx 90\%$ of the total Sm and Gd in these rocks, but very little Eu (Bea, 1996). Progressive accumulation of feldspars could also be invoked; however petrographic evidence is lacking and furthermore, CaO, Sr, Ba and Eu depletion can only be accounted for by plagioclase and K-feldspar fractionation but not accumulation.

This fractionating assemblage is in accordance with petrographic relationships between essential minerals which show that plagioclase, biotite and K-feldspar dominate the early stages of crystallization while quartz and muscovite dominate the late stages. A similar crystallization sequence is obtained experimentally by Scaillet *et al.* (1995) in the same type of compositions. However, an important difference between NAB and JB should be pointed out: in the NAB most of the biotite crystallizes simultaneously with K-feldspar whereas in the JB biotite is always an early liquidus phase found as inclusions in all the other essential minerals. This different crystallization sequence may account for the lack of parallelism in the Li and Rb trends (see Fig. 4) observed between the NAB and the JB. Early crystallization of biotite indicates high water contents in the melt (Maaløe and Wyllie, 1975; Naney, 1983; Scaillet *et al.*, 1995).

Petrogenetic model

Field and geochemical evidence reveal that formation of the NAB and JB is accomplished through the emplacement of succesive magma pulses as attested by the existence of intrusive contacts and lack of geochemical affinity between central and external units in both batholiths. An explanation for the geochemical differences between central and external units is not yet available and constitutes the main objective of our ongoing investigations (Menendez, in prep; Ramirez, in prep). This subject has already been studied in similar granitic complexes of the Central-Iberian Zone (Corretgé *et al.*, 1985; Holtz, 1989; Vigneresse and Bouchez, 1997) which indicate that units with contrasting geochemical relationships correspond to unrelated magma batches, probably generated from distinct source rocks.

Compositional trends within external units of the NAB and JB are consistent with fractional crystallization of the minerals that have been identified as early phases from petrographic observations, i.e. plagioclase, biotite and K-feldspar, together with the accessories mainly included in biotite (zircon, monazite $\pm$ apatite). Imperfect liquid-solid segregation (most samples are a mixture of solid + melt) precludes the observation of cumulates. Other examples of well-studied peraluminous granites evolving through fractional crystallization processes are the Sweetwater Wash pluton in California (Mittlefehldt and Miller, 1983), the Gangotri pluton in the Himalaya (Scaillet *et al.*, 1990), the Pedrobernardo pluton of central Spain (Bea *et al.*, 1994*a*) and the Hall Canyon pluton of California (Mahood *et al.*, 1996).

In the absence of a detailed isotopic study, source rocks for the granites that compose the external units of the NAB and JB cannot be identified. Nevertheless, both mineralogy (biotite, muscovite $\pm$ sillimanite, cordierite, andalusite and tourmaline) and whole-rock compositions (strongly peraluminous (A/CNK>1.1), CaO <1.5%, FeOt+MgO+TiO_2 <3%, high P_2O_5 and low Sr contents) clearly favour a peraluminous metasedimentary source. Considering the results of this study as well as those of Corretgé *et al.*, (1985) and Vigneresse and Bouchez (1997) on the Cabeza de Araya pluton, we suggest that the Araya batholiths of SW Iberia owe their compositional variability to assemblage of magmatic pulses generated from distinct source rocks, and further evolution within pulse by crystal fractionation processes.

Acknowledgements

The following are acknowledged: Javier Fernandez and Antonio Acosta for their help during field work and useful comments; Richard Wilson, Fernando Bea and Axel Gerdes for their revision of a first draft of this paper; Pilar Montero and Sidel Grundvig for their help with

the analytical work; and Ben Wilkinson and an anonymous referee for editorial.

References

Arth, J.G. (1976) Behaviour of trace elements during magmatic processes - a summary of theorical models and their applications. *J. Res. U.S. Geol. Surv.* **4**, 41–7.

Bea, F. (1993) Aluminosity dependent fractionation patterns in differentiated granite-leucogranite systems. *EOS (Trans. Amer. Geophys. Union)* April 20, p. 343 (abstract).

Bea, F. (1996) Residence of REE, Y Th and U within granite rocks. Implications for the chemistry of crustal melts. *J. Petrol.*, **37**, 521–52

Bea, F., Sanchez González de Herrero, J.G. and Serrano Pinto, M. (1987) Una compilación geoquímica (elementos mayores) para los granitoides del macizo Hespérico. In *Geologia de los granitoides y rocas asociadas del macizo Hespérico.* (F. Bea *et al.*, eds). Ed. Rueda, 87–193.

Bea, F., Pereira, M.D., Corretgé, L.G. and Fershtater, G.B. (1994a) Differentiation of strongly peraluminous, perphosphorous granites: The Pedrobernardo pluton, central Spain. *Geochim. Cosmochim. Acta,* **58**, 2069–27.

Bea, F., Pereira, M.D. and Stroh, A. (1994*b*) Mineral/leucosome trace element partitioning in a peraluminous migmatite (a laser ablation ICP-MS study). *Chem. Geol.*, **117**, 291–312.

Benard, F., Moutou, P. and Pichavant, M. (1985) Phase relations of tourmaline leucogranites and the significance of tourmaline in silicic magma. *J. Geol.*, **93**, 271–91.

Chappell, B.W., White, A.J.R. and Wyborn, D. (1987) The importance of residual material (restite) in granite petrogenesis. *J. Petrol.*, **28**, 1111–38.

Clarke, D.B. (1992) *Granitoid Rocks*. Chapman-Hall, 283 pp.

Clemens, J.D. and Vielzeuf, D. (1987) Constraints on melting and magma production in the crust. *Earth Planet. Sci. Lett.*, **86**, 287–306.

Corretgé, L.G. (1983) Las rocas graníticas y granitoides del Macizo Hespérico. En: *Libro Jubilar J.M. Ríos, Geología de España* I, 569–92. I.G.M.E.

Corretgé, L.G., Bea, F. and Suárez, O. (1985) Las características geoquímicas del batolito de Cabeza de Araya (Cáceres, España): implicaciones petrogenéticas. *Trab. Geol. Univ. Oviedo*, **15**, 219–38.

Deniel, C., Vidal, P., Fernández, A. *et al.* (1987) Isotopic study of the Manaslu granite (Himalaya, Nepal); inferences on the age and source of the Himalayan leucogranites. *Contrib. Mineral. Petrol.*, **96**, 78–92.

Díez Balda, M.A. (1986) *El Complejo Esquisto-Grauváquico, las Series Paleozoicas y la Estructura Hercínica al Sur de Salamanca.* Universidad de Salamanca.

Díez Balda, M.A., Martínez Catalán, J.R. and Ayarza Arribas, P. (1995) Syn-collisional extensional collapse parallel to the orogenic trend in a domain of steep tectonics: the Salamanca Detachment Zone (Central Iberian Zone, Spain). *J. Struct. Geol.*, **17**, 163–82.

Hanson, G.N. (1989) An approach to trace element modelling using a simple igneous system as an example. Geochemistry and Mineralogy of REE. *Reviews in Mineralogy,* **21**, 79–97.

Holtz, F. (1989) Importance of melt fraction and and crustal rock composition in crustal genesis - the example of two granitic suites of Northern Portugal. *Lithos*, **24**, 21–35.

Julivert, M., Fontbote, J.M., Ribeiro, A. and Conde, L. (1974) Mapa Tectónico de la Península Ibérica y Baleares. Escala 1: 1 000 000. *IGME,* pp. 1–101.

Le Maitre, R.W. (1982) *Numerical Petrology*. Elsevier. Amsterdam, 281pp.

López Plaza, M. and Martínez Catalán, J.R. (1987) Síntesis estructural de los granitoides del Macizo Ibérico. In *Geología de los Granitoides del Macizo Hespérico* (F. Bea *et al.*, eds.). 195–210.

Maaløe, S. and Wyllie, P.J. (1975) Water content of a granitic magma deduced from the sequence of crystallization determined experimentally with water undersaturated conditions. *Contrib. Mineral. Petrol.*, **52**, 175–91.

Mahood, G.A., Nibler, G.E. and Halliday, A.N. (1996) Zoning patterns and petrologic processes in peraluminous magma chambers: Hall Canyon Pluton, Panamint Mountains, California. *GSA Bull.*, **108**, 437–53.

Martínez Catalán, J.R. (1990) A non-cylindrical model for the northwest Iberian allochthonous terranes and their equivalents in the Hercynian belt of Western Europe. *Tectonophysics*, **179**, 253–72.

McCarthy, T.S. and Hasty, R.A. (1976) Trace element distribution patterns and their relationship to the crystallization of granitic melts. *Geochim. Cosmochim. Acta*, **40**, 1351–8.

Miller, C.F. (1985) Are peraluminous magmas derived form pelitic sedimentary sources?. *J. Geol.*, **93**, 673–89.

Mittlefehldt, D. and Miller, C.F. (1983) Geochemistry of the Sweetwater Wash Pluton, California: Implications for anomalous trace element behaviour during differentiation of felsic magmas. *Geochim. Cosmochim. Acta*, **47**, 109–24.

Montel, J.M. and Vielzeuf, D. (1997) Partial melting of metagreywackes part II. Compositions of minerals and melts. *Contrib. Mineral. Petrol.*, **128**, 176–96.

Nancy, M.T. (1983) Phase equilibria of rock-forming ferromagnesian silicates in granitic systems. *Amer. J. Sci.*, **283**, 993–1033.

Nash, W.P. and Crecraft, H. R. (1985) Partition coefficients for trace element in silicic magmas. *Geochim. Cosmochim. Acta.*, **49**, 2309–22.

Patiño Douce, A.E. and Johnston, A.D. (1991) Phase equilibria and melt productivity in the pelitic system: implications for the origin of peraluminous granitoids and aluminous granulites. *Contrib. Mineral. Petrol.*, **107**, 202–18.

Ramirez, J.A. (1996) *Estudio petrológico, geoquímico e isotópico del batolito de Jálama (N. de Extremadura)*. PhD thesis. Univ. de Granada, Spain.

Ribeiro, A. (1974) Contribution à l'etude tectonique de Tras-os-Montes Oriental. *Mem. Serv. Geol. Port.*, **24**, 1–168.

Rodríguez Alonso, M.D., (1985) *El complejo esquisto grauváquico y el Paleozoico en el centro-oeste español*, Universidad de Salamanca. 174 pp.

Rollinson, H. (1993) *Using Geochemical Data: Evaluation, Presentation, Interpretation*. Longman. 352 pp.

Scaillet, B., France-Lanord, C. and Le Fort, P. (1990) Badrinath-Gangotri plutons (Garwahl, India): petrological and geochemical evidence for fractionation processes in a high Himalayan leucogranite. *J. Volcanol. Geotherm. Res.*, **44**, 163–8.

Scaillet, B., Pichavant, M. and Roux, J. (1995) Experimental crystallization of leucogranite magmas. *J. Petrol.*, **36**, 663–705.

Serrano Pinto, M., Casquet, C., Ibarrola, E., Corretgé, L.G. and Portugal Ferreira, M. (1987) Sintese geocronologica dos granitos do maciço hesperico. In *Geologia de los Granitoides del Macizo Hespérico*. (F. Bea *et al.*, eds). Madrid Rueda, 69–86.

Shearer, C.K., Papike, J.J. and Laul, J.C. (1987) Mineralogical and chemical evolution of a rare-element granite-pegmatite system: Harney Peak Granite, Black Hills, South Dakota. *Geochim. Cosmochim. Acta*, **51**, 473–86.

Suárez Rodríguez (1985) *Petrografía, blastesis y deformación en la aureola de contacto del plutón de Nisa Alburquerque*. Tesis de licenciatura. Univ. Oviedo.

Vigneresse, J.L. and Bouchez, J.L. (1997) Successive granitic magma batches during pluton emplacemente: the case of Cabeza de Araya (Spain). *J. Petrol.*, **38**, 1767–76.

Wall, V.J., Clemens, J.D. and Clarke, D.B. (1987) Models for granitoid evolution and source composition. *J. Geol.*, **95**, 731–49.

Wilkinson, L. (1989) SYSTAT: The system for statistics. Evanson, IL, 638p.

Williamson, B.J., Shaw, A., Downes, H. and Thirlwall, M.F. (1996) Geochemical constraints on the genesis of Hercynian two-mica leucogranites from the Massif Central, France. *Chem. Geol.*, **127**, 25–42.

Zen, E. (1988) Phase relations of peraluminous granitic rocks and their petrogenetic implications. *Ann. Rev. Earth Planet. Sci.*, **16**, 21–51.

[*Manuscript received 18 August 1997; revised 21 April 1998*]